Soft Matter

Accepted Manuscript

ROYAL SOCIETY OF CHEMISTRY

www.rsc.org/softmatter

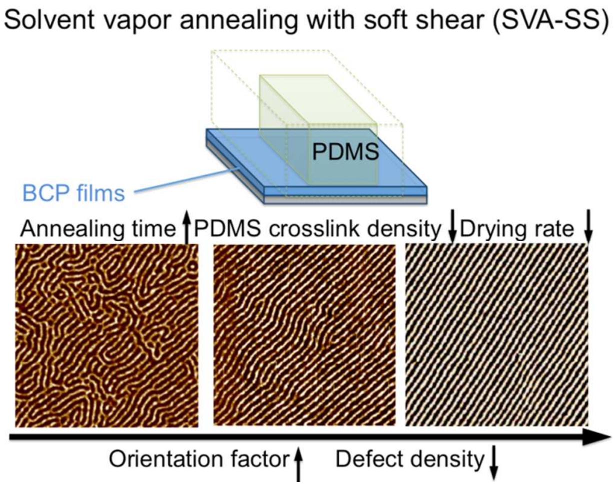
Solvent vapor annealing with soft shear (SVA-SS)
PDMS
BCP films
Annealing time ↑
PDMS crosslink density ↓
Drying rate ↓
Orientation factor ↑
Defect density ↓

Soft Matter RSCPublishing

ARTICLE

Cite this: DOI: 10.1039/x0xx00000x

Received 00th January 2012,
Accepted 00th January 2012

DOI: 10.1039/x0xx00000x

www.rsc.org/

A generalized method for alignment of block copolymer films: Solvent vapor annealing with soft shear

Zhe Qiang[a], Yuanzhong Zhang[a], Jesse Groff,[b] Kevin A. Cavicchi[a]* and Bryan D. Vogt[a]*

ABSTRACT. One of the key issues associated with the utilization of block copolymer (BCP) thin films in nanoscience and nanotechnology is control of their alignment and orientation over macroscopic dimensions. We have recently reported a method, solvent vapor annealing with soft shear (SVA-SS), for fabricating unidirectional alignment of cylindrical nanostructures. This method is a simple extension of the common SVA process by adhering a flat, crosslinked poly(dimethylsiloxane) (PDMS) pad to the BCP thin film. The impact of processing parameters, including annealing time, solvent removal rate and the physical properties of the PDMS pad, on the quality of alignment quantified by the Herman's orientational factor (S) is systematically examined for a model system of polystyrene-*block*-polyisoprene-*block*-polystyrene (SIS). As annealing time increases, the SIS morphology transitions from isotropic rods to highly aligned cylinders. Decreasing the rate of solvent removal, which impacts the shear rate imposed by the contraction of the PDMS, improves the orientation factor of the cylindrical domains; this suggests the nanostructure alignment is primarily induced by contraction of PDMS during solvent removal. Moreover, the physical properties of the PDMS controlled by the crosslink density impact the orientation factor by tuning its swelling extent during SVA-SS and elastic modulus. Decreasing the PDMS crosslink density increases S; this effect appears to be primarily driven by the changes in the solubility of the SVA-SS solvent in the PDMS. Furthermore, this change can significantly impact the defect density of the thin film. With this understanding of the critical processing parameters, SVA-SS has been applied to align a wide variety of BCPs including polystyrene-*block*-polybutadiene-*block*-polystyrene (SBS), polystyrene-*block*-poly(N,N-dimethyl-*n*-octadecylammonium p-styrenesulfonate) (PS-*b*-PSS-DMODA) , polystyrene-*block*-polydimethylsiloxane (PS-*b*-PDMS) and polystyrene-block-poly(2-vinlypyridine) (PS-*b*-P2VP). These results suggest that SVA-SS is a generalizable method for the alignment of BCP thin films.

Introduction

The spontaneous formation of nanostructured materials *via* self-assembly of the block copolymers (BCP) has received increasing interest for a wide variety of applications including high lithium-ion conductivity for batteries[1, 2]; organic optoelectronics[3, 4]; directed assembly for next generation lithography in microelectronics[5-7]and filtration membranes[8, 9]. These applications exploit the self assembly of BCPs into well defined nanostructures[10], which are well understood in bulk systems[11, 12] with BCP morphologies determined primarily by the Flory-Huggins interaction parameter between different blocks, χ; the degree of polymerization, N, and the segmental volume fraction (f_i) of the block, where the driving force for the microphase separation is χN[12-14]. In thin films, additional factors such as the film thickness, surface energies (both substrate energy and free surface energy) and substrate chemistries can influence the morphology and orientation[15-17].

However, these BCP nanostructures are generally kinetically controlled due to the limited mobility of the BCP. Moreover, defect elimination is difficult to obtain when solely utilizing thermal annealing[18] and the ordering kinetics are further suppressed in thin films[19]. For some BCPs, even modest ordering can pose some problems if the glass transition temperature (T_g) is greater than temperatures where degradation may occur[20]. Moreover, chain mobility is a significant impediment to ordering if large domain spacings are desired[21] due to its $N^{2/3}$ scaling[22]. Solvent vapor annealing (SVA) provides an effective alternative approach to order BCP films, where the solvent swells the BCP film, effectively reducing T_g and enhancing chain mobility.[23, 24] This swelling behavior can significantly decrease χN through screening of unfavorable interactions[25], thus it is possible to disorder the film during SVA if sufficiently aggressive conditions are utilized. SVA can also impact the morphology by selectively swelling one component to effectively tune the volume fraction (f_i).[26, 27] Solvent mixtures can provide a route to produce neutral wetting conditions at the film surface to promote perpendicular orientation of cylinders.[28] Similarly, the BCP domain spacing and morphology orientation can be impacted by solvent vapor pressure[29,30] and the solvent removal rate.[31]

Although both thermal annealing and SVA enable ordering the BCP domains, the self-assembled structures are not aligned over macroscopic dimensions with the film consisting of randomly oriented grains[10]. To provide this longer range alignment, numerous methods have been developed such as external fields (electrical fields or magnetic fields)[32-34]; epitaxy[35]; mechanical shear[36, 37]; zone casting[38]; cold zone annealing (CZA)[39-41] and micro-patterned substrates[42, 43]. However, these methodologies generally require specialized equipment or substrates, which limits the ability to generally adopt these methods due to the costs involved. Jung and coworkers reported using a pre solvent-swollen polymer gel pad (PDMS) for aligning the high-χ BCPs in an extremely short time with movement of the pad across the surface and the best alignment was obtained when using a patterned substrate[44]. This method still requires a methodology for moving the PDMS pad across the surface of the film. Recently, we demonstrated a method to fabricate highly aligned BCP thin films based upon simple modification of the commonly utilized solvent vapor annealing (SVA) process with a soft, flexible elastomeric capping pad (PDMS)[45] for cylinder-forming polystyrene-*block*-polyisoprene-*block*-polystyrene (SIS) films. Due to swelling of the elastomer pad, a soft shear (SS) is produced during drying due to an evaporation front that aligns the BCP domains. The drying front is a result of the directional flow of dry air through the cell over the sample; the diffusion of solvent out of the PDMS pad and the non-centered alignment of PDMS with respect to the air flow results in one corner of the rectangular pad drying first, which through propagates diagonally across the PDMS as defined by its dimensions.[45] This technique is analogous to the CZA-SS method,[40] where a sharp temperature gradient, rather than solvent gradient, provides the driving force for shear alignment.. By slightly offsetting the PDMS edge to dry gas inlet purposefully, the direction of the alignment of the self-assembled cylinders can be controlled by the shape and placement of the elastomer on the film due to the directional drying. This methodology is applicable to a wide range of film thicknesses from monolayer to micron thick films. However, the generality of this technique for the alignment of BCP films is not clear.

Here, we identify processing parameters that impact the alignment of the BCP films to understand how to extend this SVA-SS method from SIS to other BCP systems. The SVA exposure time, drying rate and the physical properties of the PDMS all impact the efficacy of alignment. The orientation factor can be improved and the defect density decreased by decreasing the crosslink density of the PDMS, which increases the solvent solubility (swelling ratio); increasing SVA-SS time; or decreasing the solvent removal rate. This provides further insight into the alignment mechanism associated with SVA-SS. With this knowledge, we have successfully extended SVA-SS to align polystyrene-*block*-polybutadine-*block*-polystyrene (SBS), polystyrene-*block*-poly(N,N-dimethyl-n-octadecylammonium p-styrenesulfonate) (PS-*b*-PSS-DMODA), polystyrene-*block*-poly(dimethylsiloxane) (PS-*b*-PDMS) and polystyrene-block-poly(2-vinylpyridine) (PS-*b*-P2VP). With proper selection of processing conditions, SVA-SS is a generalizable methodology for the alignment of BCP films.

Experimental Section

Materials

Chloroform (>99.8%) and cyclohexane (>99%) were purchased from Alfa Aesar. Toluene (ACS grade) and tetrahydrofuran (THF) (>99%) were purchased from Sigma-Aldrich. Methyl-ethyl-ketone (MEK) (>99%) and hexane (>99%) were obtained from Fisher Scientific. Styrene was purified using a basic alumina column in order to remove the polymerization inhibitor. All other chemicals were used as received. Polystyrene-*block*-polyisoprene-*block*-polystyrene (SIS) copolymer (Kraton 1164P), containing 29 vol% polystyrene and polystyrene-*block*-polybutylene-*block*-polystyrene (SBS) copolymer (Kraton D1116A), containing 23 vol% polystyrene were obtained from Kraton Polymers. PS-*b*-PSS-DMODA (M_n=10.2 kg/mol, f_{PS}=0.67, PDI=1.26)[30] and PS-*b*-PDMS (M_n=46.1 kg/mol, f_{PDMS}=0.23, PDI=1.21)[46] were synthesized by RAFT polymerization as previously reported. PS-*b*-PMMA (M_n=47.5 kg/mol, f_{PS}=0.74, PDI=1.07) and PS-*b*-P2VP (58 kg/mol, f_{PS}=0.71, PDI=1.07) were purchased from Polymer Source Inc. The crosslink density of PDMS (Sylgard 184, Dow Corning) was varied using the base to curing agent ratios. Four different ratios (w/w) were evaluated: 5:1; 10:1; 15:1; and 20:1. The PDMS base and curing agent were first physically mixed by hand at the desired ratio. Once mixed, the mixture was degased under vacuum at ambient temperature for 15 min and then poured onto a flat glass plate to create an approximately 0.5 mm thick film. Subsequently, the PDMS was allowed to cure at room temperature for 1 h, followed by cure at 120 °C for 2 h. The nomenclature utilized to identify these PDMS samples is PDMS-*x*, where *x* is the mass ratio of base to curing agent. The cured PDMS was then cut into ca. y x y cm pads to act as soft capping layers for the BCP films.

Thin film preparation and processing

(100)-oriented silicon wafers (University Wafer) were used as substrates. The wafers were cleaved with a diamond scribe into approximately 3 cm × 3 cm pieces and were cleaned using ultraviolet-ozone (UVO, Jelight Company Inc., Model No. 42) for 2 h. SIS, SBS and PS-*b*-PMMA thin films were spun cast from 2 wt% solution in toluene at 3500 rpm for 1 min. PS-*b*-PSS-DMODA thin films were spun cast from 2 wt% solution in MEK at 3500 rpm for 1 min. PS-*b*-PDMS thin films were spun cast from 2 wt% solution in benzene at 3500 rpm for 1 min. PS-*b*-P2VP thin films were spun cast from 2 wt% solution in THF at 3500 rpm for 1 min. In order to directly measure the swelling of PDMS, PDMS-20 thin films were spun cast from 5 wt% solids solution in hexane at 3500 rpms for 1 min, followed by curing at 120° C for 2 h.

For the SVA-SS process, PDMS pads approximately 0.5 mm thick were laminated to the BCP films with the PDMS fully wetting the BCP films prior to SVA. The standard SVA conditions utilized for the PDMS pads of different crosslink density were exposure to nearly saturated toluene vapor for 2 h using mass flow controllers (MKS-146C-FF000-1) flowing dry air at 800 mL/min through liquid toluene. Solvent removal was performed by flow of neat air at 25 mL/min for 30 min. For investigating the effect of SVA time on the morphology, the SIS films capped with the PDMS pad were then exposed for 5 min - 120 min to nearly saturated toluene vapor at 800 mL/min. The films were dried for 30 min using neat dry air flowing at 25 mL/min. Additionally, the effect of solvent removal rate on the morphology was examined by varying the flow rate of the dry air from 5 mL/min to 800 mL/min after the SIS films were annealed in toluene vapor for 2 h at the standard condition. For extending SVA-SS to other BCPs, SBS; PS-*b*-PSS-DMODA; PS-*b*-PMMA; PS-*b*-PDMS and PS-*b*-P2VP thin films were exposed to saturated selected solvent vapor for 2 h and dried at 25 ml/min for 30 min.

Characterization

The swelling behavior of the PDMS pad was measured according to the method reported by Whitesides[47]: simply placing a PDMS strip in toluene for 2 h and then measuring the change in the dimensions (e.g. length) of the solid while the PDMS is still submersed in the toluene in the liquid phase. The degree of swelling is expressed by the swelling ratio: $S=L/L_0$, where L is the length of PDMS in the toluene and L_0 is the original length of PDMS before swelling.

The film thickness of the SIS and PDMS thin films was determined using variable angle spectroscopic ellipsometry (VASE, J.A.Woollam Co., M-2000) in a wavelength range from 246 nm to 1689 nm with three angles of incidence: 65°, 70° and 75°. The ellipsometric angles (Δ and Ψ) were fit using a recursive model consisting of silicon, an interface layer, a SiO_2 layer (to represent the native oxide)[48] and a Cauchy layer to describe the polymeric films. The swelling and deswelling of SIS and PDMS thin films by toluene vapor were measured *in-situ* by VASE at 70° using a custom cell with quartz windows. Atomic force microscopy (AFM, Dimension ICON, Veeco) in tapping mode at 0.5 Hz was used to investigate the surface morphology of the films after SVA using PPP-NCC-50 tips (Nanosensors). In order to determine the mechanical properties of PDMS, the PDMS was cut into 8 cm × 3 cm strip for uniaxial tensile testing using a texture analyzer (Texture Technologies Corp., TA-XP PLUS). A total of twenty PDMS samples for each of the four crosslink densities were stretched at a rate of 0.05 mm/s. The elastic modulus of the polymers was determined from the slope of the linear regression of the stress-strain curves from 0–6 % strain, which is in the linear elastic regime.

Results and discussion

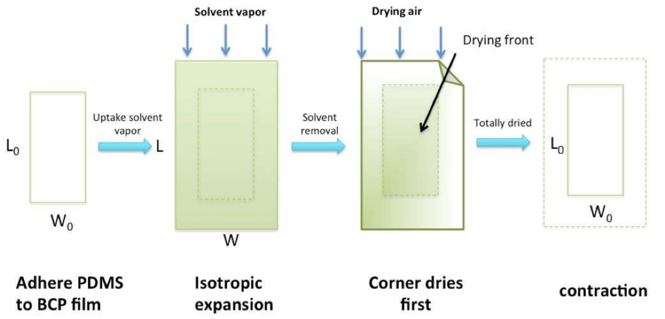

Figure 1. Schematic of the SVA-SS process. Swelling and deswelling of the adhered PDMS pad leads to shear alignment of the BCP microdomains.

Figure 1 schematically illustrates the standard SVA-SS process: A rectangular PDMS pad is adhered to the top of BCP film before SVA-SS. Both the PDMS and BCP are swollen by uptake of the solvent vapor, which plasticizes the BCP to enhance its mobility and enable ordering. Subsequently, a directional evaporation front is established during solvent removal from the dry air stream, which leads to the development of a shear field and provides alignment of the BCP domains along the diagonal direction of the PDMS pad. The direction for the aligned BCP domains can be controlled simply by the shape of the PDMS pad and its orientation on the substrate relative to the flow direction for the dry air. From diffusion arguments, the initial drying of a corner of the PDMS is expected; the propagation of this drying across the PDMS proceeds in a direction that is parallel to the diagonal across the rectangle of the PDMS. This corner first drying is consistent with the uneven evaporation front for a swollen PDMS exposed to the air.[47] We define the direction of the SS to be the diagonal across the rectangle as denoted by the arrow illustrated in Figure 1 for the directional drying.

For the SVA-SS process to be effective, the SIS film must be swollen by the toluene to provide mobility. From ellipsometry measurements ca. 2 min is required for both the SIS film and PDMS-20 thin film to reach equilibrium swelling state (See ESI). However, during SVA-SS, the PDMS pad (0.5 mm; much thicker than PDMS-20 thin film, 503 nm) acts as an effective diffusion barrier for the toluene and slows the solvent uptake into the SIS as this diffusion controlled equilibration is dependent on both the intrinsic diffusivity and the transport path length, so the time exposed to the toluene vapor will be important. Figure 2A illustrates the surface nanostructure of the SIS film after SVA-SS for 15 min using PDMS-20. The surface morphology consists of short rods without any preferential orientation as evidenced by the FFT inset, which is similar to the as-cast state (see ESI). Increasing the SVA exposure time to 30 min results in slight alignment of the cylinders (Figure 2B), while cylinders also become longer on average. The FFT inset (Figure 2B) illustrates the slight alignment with the crescents associated with preferred direction for the cylindrical nanostructures. The SS direction provided in the figures is that from geometry of the PDMS pad, which can be assessed by alignment of the sample during the AFM measurements to a trough[45] in the films that develop at the edges of the PDMS after SVA-SS. Further increasing the annealing time to 45 min (Figure 2C) produces a signifcant improvement in the alignment. However, there remains a significant defect density that degrade the quality of the orientation. The alignment is further improved with a signficant decrease in the defects in the ordered structure by increasing the annealing time to 1 h (Figure 2D). The streaks (both first order and second order peaks) from the FFT of the micrographs narrow and thin towards points, which is consistent with the increased alignment of SIS thin film nanostrcuture along with the SVA-SS direction.

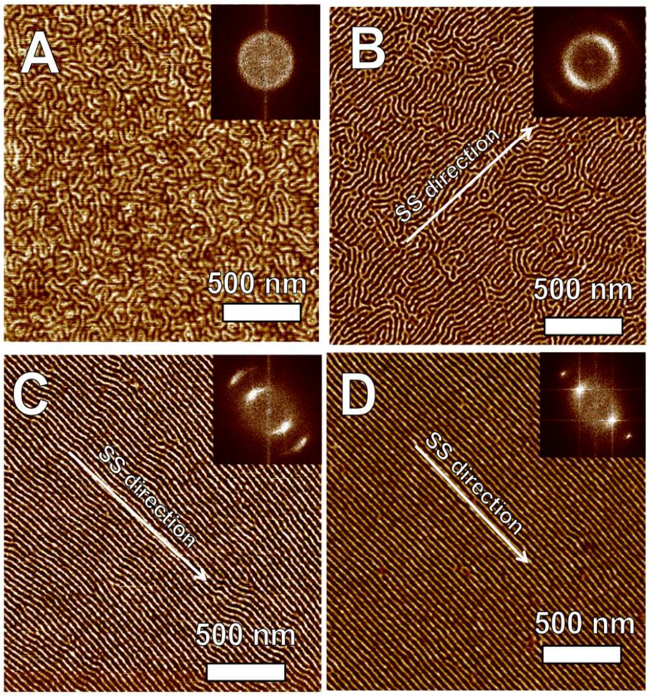

Figure 2. AFM phase images for SIS films SVA-SS annealed using PDMS-10 pad for (A) 15 min; (B) 30 min; (C) 45 min and (D) 60 min.

In order to quantify the orientation degree of these nanostructured SIS thin films as a function of annealing time, the FFTs from the AFM micrographs are analyzed as a function of azimuthal angle to calculate the Hermans orientation factor, S[51], as:

$$S = \frac{3 < cos^2\emptyset > -1}{2}$$

where ϕ is the azimuthal angle and $\langle \cos^2 \phi \rangle$ is the average of $\cos^2 \phi$ based on the intensity of the FFT at a given azimuthal angle, I(ϕ), calculated as

$$< cos^2\emptyset >= \frac{\sum_{\emptyset=0^\circ}^{90^\circ} I(\emptyset) sin\emptyset cos^2\emptyset}{\sum_{\emptyset=0^\circ}^{90^\circ} I(\emptyset) sin\emptyset}.$$

Figure 3 shows the orientation factor for these SIS films annealed by SVA-SS for different times. For the films annealed for 15 min, there is no preferred alignment direction for the nanostructures, so S=0. For the weakly aligned SIS films (Figure 2B), the orientation factor S is around 0.28. Once the annealing time increases to 45 min and 1 h, the orientation factor S increases significantly to 0.83 and 0.91 respectively. This improvement in the alignment of cylinders is consistent with tranformation from the micrographs consisting some randomly oriented rods to the well-aligned cylindrical structures from AFM. For longer time, there is no statistical change in *S*. This suggests that the SIS film reaches equilibrium swelling (and potential rearrangements associated with ordering) in 45-60 min when using a 0.5 μm thick PDMS pad.

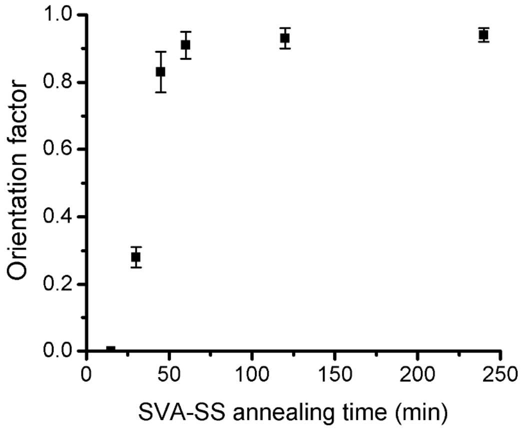

Figure 3. Orientation factor of SIS films using PDMS-10 as elastomer pad as a function of SVA-SS annealing time

For other alignment techniques such as applied mechanical shear[52] or CZA,[39, 41] the rate at which the alignment force is applied to the film is critical. Thus for SVA-SS, the rate of drying induced by air flow impacts the rate at which the soft shear is applied. To first illustrate how the flow rate of dry air impacts the contraction of the PDMS, a PDMS-20 thin film is monitored *in-situ* using ellipsometry (Figure 4) after the film is pre-swollen from 513 nm to 742 nm by toluene vapor.

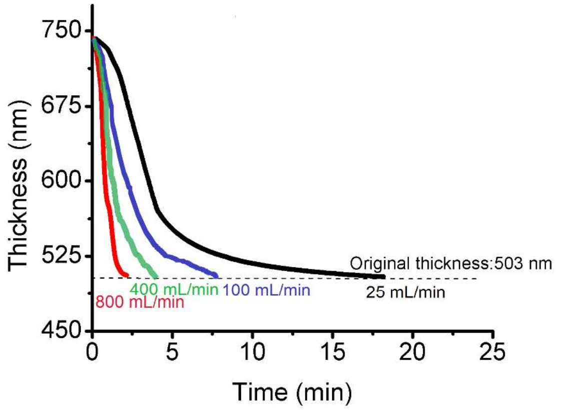

Figure 4. Film thickness profile for PDMS-20 annealed with toluene vapour at a constant swollen thickness at different solvent removal rates associated with the flow rate of the dry air.

Figure 4 shows as the flow rate of dry air is decreased, the PDMS-20 film more gradually returns to its original thickness. When the drying air flow rate is 25 mL/min (typical procedure), the thickness of PDMS film decreases at approximately 0.5 nm/s for first 6 min and subsequently the PDMS film thickness decrease is even slower as the original thickness is approached. When the air flow is increased to 100 mL/min, the PDMS thickness decreases at 0.8 nm/s. By further increasing the flow rate to 400 mL/min and 800 mL/min, the PDMS film shrinks at approximately 1.3 nm/s and 1.8 nm/s, respectively. The fastest flow rate (800 mL/min) shrinks the PDMS 4 times faster the slowest conditions (25 mL/min), which shows the controllable contraction rate by tuning the dry air rate.

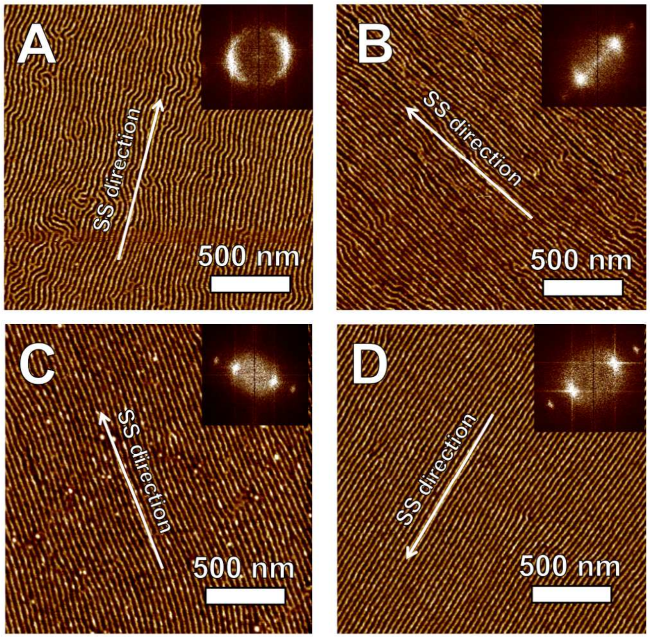

Figure 5. AFM phase images of the SVA-SS annealed SIS films at different PDMS-20 deswell rate. (A) 800mL/min; (B) 400mL/min; (C) 100mL/min and (D) 25 mL/min.

Figure 5 illustrates how the drying conditions impact the surface morphology of SIS films. Under the fastest drying rate (800 mL/min; Figure 5A), the AFM phase images consists of curved-cylinders aligned along the SVA-SS direction and some random short rods. This poor alignment of cylinders is attributed to the limited the time for aligning the cylinders associated with the fast shear rates, which is similar to the CZA-SS where the orientation decreases significantly when hot zone moves too fast[40]. By decreasing the drying air rate to 400 mL/min (Figure 5B) and 100 mL/min (Figure 5C), the alignment of cylindrical structures are enhanced along the SVA-SS direction; however, there still are some defects presented in the ordered structures. Further decreases the drying rate (25 mL/min, Figure 5D), the SIS film shows well-aligned cylinders, which is consistent with the previous results[45].

Figure 6 illustrates the orientation factor of the SIS films after SVA-SS under different drying rate and ranges from S=0.38 to S=0.91 over the range of drying rates. The increase of the alignment by decreasing the drying rate proves the alignment of structure is mostly induced by deswelling of the PDMS pad.

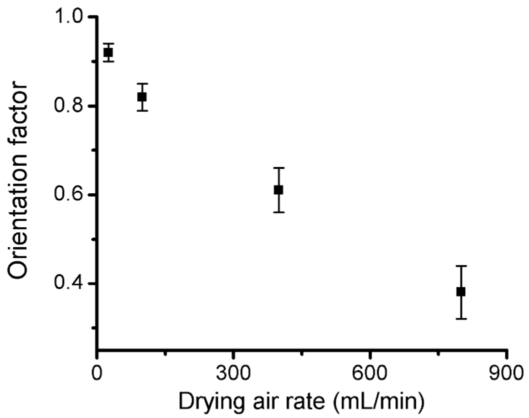

Figure 6. Orientation factor of the SVA-SS annealed SIS film using PDMS-20 pad as a function of drying air rate.

In addition to the drying rate, the total shear strain produced by the PDMS pad during drying also plays a critical role for perfection in nanostructural alignment. Although the vapor pressure of the toluene could tune the PDMS swelling, it will also impact the plasticization of the SIS film, so the effects will not be isolated. Thus, for investigating how the swelling ratio of the PDMS pad affects the alignment of SIS thin films, four different crosslink density PDMS pads were fabricated based upon varying the mass ratio of PDMS base to curing agent. For an elastomer network, the swelling and elastic modulus of the network are closely related. Figure 7 illustrates the elastic modulus and swelling ratio of PDMS with different crosslink density. The modulus decreases by nearly an order of magnitude as the PDMS base to curing agent ratio increases from 5 to 20 (3.1 MPa and 0.65 MPa, respectively). This change in the elastic modulus of PDMS is consistent with previous report for development of PDMS with tunable mechanical properties[53].

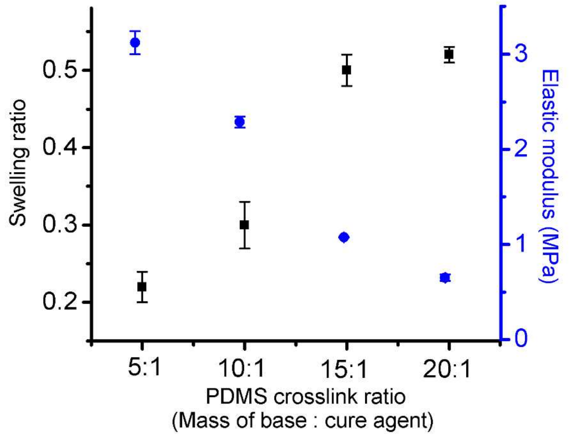

Figure 7. Elastic modulus (•) and swelling ratio (■) of PDMS as a function of its crosslinking ratio of base to curing agent.

For the PDMS-5, it swells around 22% in toluene solvent. Once the mass ratio of base to curing agent increases to 10, the PDMS swells around 30% in the toluene which is consistent with reports by Whitesides and coworkers[47]. For the PDMS-15 and PDMS-20, the swelling ratio is 50% and 52% respectively, indicating the similar swelling behavior for these two crosslink density PDMS. This 50% increase in the length is near to the swelling ratio determined for PDMS-20 thin films for toluene vapor as shown in ESI.

Figure 8 illustrates the evolution in surface morphology of the SIS films with different crosslink densities of the PDMS pad. Using the highly crosslinked PDMS (PDMS-5) (Figure 8A), there is some waviness in the cylinders and some randomly oriented nanostructures remain. The FFT yields crescents, consistent with preferred directional orientation overall, but also illustrative of the large defect density. Using PDMS-10 as the pad (Figure 8B), these cylindrical structures are better aligned compared to that obtained with PDMS-5 as the peak in FFT becomes much sharper. Further decreasing the crosslink density of PDMS pad results in highly aligned and correlated stripe pattern that persists across the film. From the FFT of the micrographs as shown in the inset in Figure 8C and Figure 8D, the alignment of the structure can be clearly seen by two orders of diffraction spots.

Figure 9 shows *S* of these SIS films as a function of the swelling ratio (PDMS crosslink density). For the SIS film capped with PDMS-5 pad, the orientation factor is only 0.67, which is attributed to the limited swelling ratio of PDMS-5 (22 %) by toluene vapor. As the swelling of the PDMS increases, the film's orientation factor increases. The orientation factor increases to 0.94 and 0.95 for the films capped with PDMS-15 and PDMS-20 pads, respectively. Thus, there appears to be a minimum threshold for swelling to obtain highly aligned ($S > 0.90$) that is greater than 35 %. The enhancement of orientation factor with the increase of PDMS swelling ratio illustrates that the local contraction of PDMS during drying provides the force for macroscale alignment of BCP nanostructures.

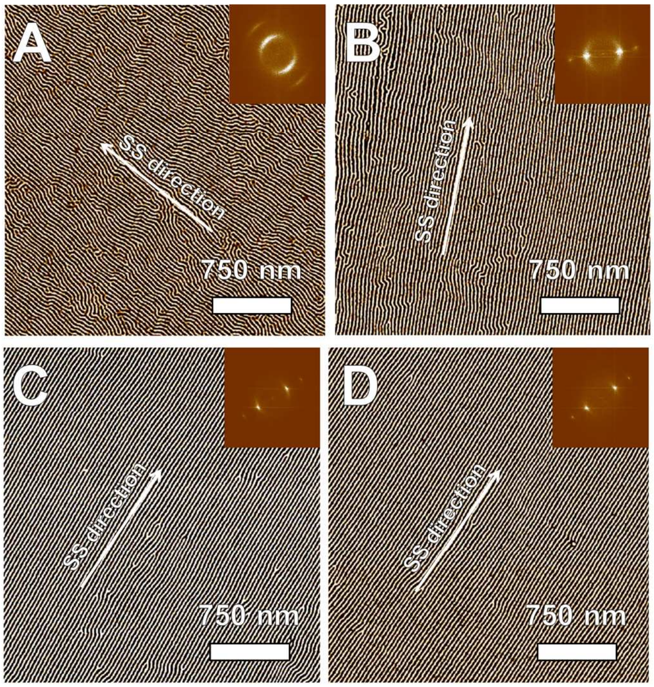

Figure 8. AFM phase images of SIS film after SVA-SS by different crosslink ratio PDMS (mass of base: cure agent) (A) 5:1; (B) 10:1; (C) 15:1; (D) 20:1.

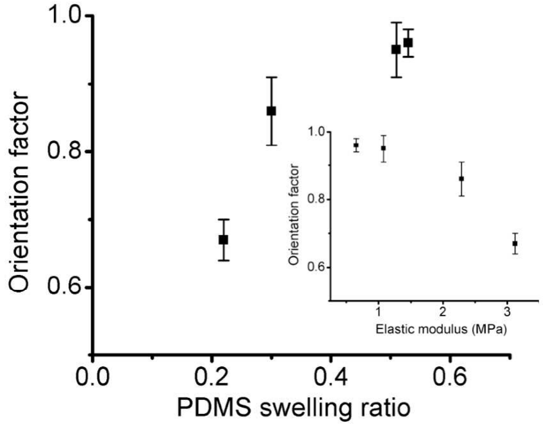

Figure 9. Orientation factor of SIS film after SVA-SS determined by AFM phase images as a function of PDMS swelling ratio. The inset is the orientation factor of SIS film after SVA-SS as a function of the elastic modulus of the PDMS pad.

To further assess the surface morphology of SVA-SS annealed SIS films with the different crosslink density PDMS pad, defects including dislocations and declinations are statistically analysed in an area of 3 μm × 3 μm. Five areas of each film are randomly selected for the defect analysis (See ESI). Figure 10 shows the average defect density (ρ) as a function of PDMS crosslink density. By increasing the crosslinker ratio of PDMS from 5 to 10, the defect density in the SIS films decreased significantly from 22 μm^{-2} to 13 μm^{-2}. Further increasing the crosslinker:base ratio of PDMS to 15 and 20, the defect density remarkably decreased to 2 μm^{-2} and 1 μm^{-}

^{2}, respectively. This dramatic reduction in defect density in the SIS films with increasing swelling ratio of PDMS pad is attributed primarily to the tendency of dislocation with opposite signs to attract and annihilate by either motion along the cylinders or across the cylinders. This behavior appears to be very similar to the defect annihilation within cylinder-forming BCP thin films on nanopatterned substrates.[54]

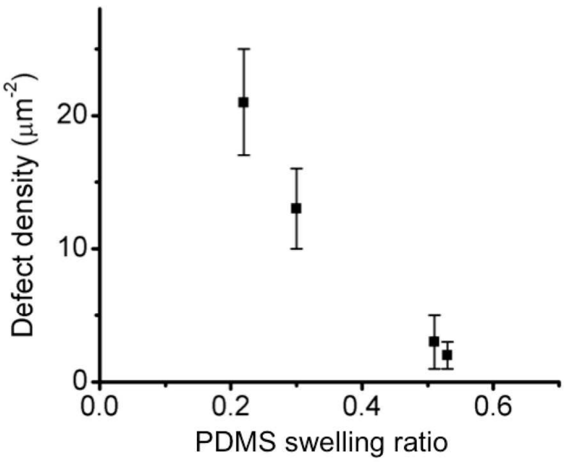

Figure 10. Defect analysis of SIS film after SVA-SS by different crosslink ratio PDMS determined by AFM.

To understand the importance of solvent selection on the alignment of BCP films by SVA-SS, hexane (selective for PS) and acetone (selective for PI) have been used for SVA-SS with the same SIS films (See ESI). Although PDMS-10 swells 38% in hexane[47], which is greater than in toluene, neither of these solvents leads to any marked improvements in the alignment of the nanostructure in these films (See ESI). It appears that a selective solvent in SVA-SS is not effective for aligning the BCP nanostructures and the solvent must swell both the BCP films for plasticization and the elastomer to provide shear strain for the alignment.

Based on the heuristics developed for solvent selection, we utilized the SVA-SS method for aligning a series of other block copolymers. In these cases, PDMS-20 is utilized along with a 2 h SVA and subsequent drying at the slow rate (25 mL/min). The common characteristic fingerprint morphology associated with modest range order cylinders of these films is observed after a standard SVA protocol without a PDMS pad in all cases (see ESI), Figure 11A shows the highly aligned stripe pattern surface morphology of the SBS film after SVA-SS using toluene vapor, which is a good solvent for both segments. Similarly, the PS-*b*-PSS-DMODA (Figure 11B) film after SVA-SS using chloroform (good solvent for PS and PSS-DMODA, PDMS swells 39% in chloroform[47]) shows unidirectional cylinders across the micrograph with sub-10 nm spacing (S = 0.92). These results show the capability of SVA-SS methods for aligning a wide range of domain sizes from sub-10 nm to at least 50 nm. For lithography applications, PS-*b*-PDMS is of great interest and can be aligned using SVA-SS method and THF vapor (good solvent for PS and PDMS, PDMS swells 34% in THF) as illustrated in Figure 11C. Interestingly, the orientation factor of these aligned nanostructures after SVA-SS is around 0.93, which is greater than the best films processed with CZA-SS (S = 0.85) method for the same PS-*b*-PDMS copolymer.[55] Figure 11D shows the surface morphology of PS-*b*-P2VP film after SVA-SS using THF (good solvent for PS and P2VP; PDMS swells 34% in THF[47]) and a majority of the cylinders are aligned along their primary axis in the SVA-SS direction. In this case, the orientation factor of PS-*b*-P2VP is significantly less than other films (0.79). We attribute this decrease in the alignment due to the lower swelling of PS-*b*-P2VP films by THF vapor (24%) than the other BCP films by their solvent pair vapors (34-39%). This decrease in swelling limits the polymer mobility for ordering even during standard SVA (See ESI). However, the application of SVA-SS to PS-*b*-P2VP film still significantly enhances the ordering and alignment when compared to the standard SVA process (see ESI).

However, PS-*b*-PMMA (See ESI) after SVA-SS using chloroform shows limited ordering. This is different from the previous results with highly aligned cylinders and may be due to the much lower χN between PS and PMMA block[56] compared to the high molecular weight SIS. In chloroform vapor, the PS-*b*-PMMA film is swollen around 35% and thus χN in the swollen state is approximately 7; this is based on the estimate of $\chi_{eff}=(1-\phi_s)^{1.6}\chi$,[□□] where χ is calculated using prior reports for PS-*b*-PMMA[56] and ϕ_s is the volume fraction of solvent in the swollen film. This calculation suggests PS-*b*-PMMA is disordered[57] when fully swollen. Thus during the solvent removal, the PS-*b*-PMMA begins to microphase separate while the PDMS deswells to produce the shear force for alignment. These two simultaneous processes do not appear to enable ordering of nanostructures after SVA-SS. It appears that the BCP should remain ordered during SVA-SS for aligning the nanostructures with SVA-SS.

Overall, there appear to be five important factors to consider in order to obtain highly aligned nanostructures: 1) Sufficient annealing time for the polymer and PDMS pad to reach equilibrium; 2) Slow drying rate of PDMS pad to enable polymer chains reorganization during shear for alignment; 3) Sufficient shear strain from the PDMS to align the nanostructure; 4) Solvent should be good for all components including the elastomer pad and BCP segments; and 5) The BCP films should remain ordered during SVA-SS.

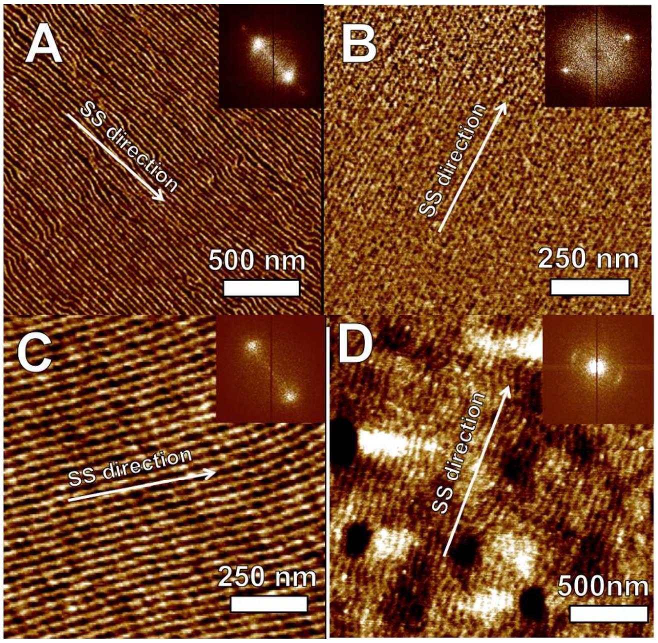

Figure 11. AFM phase images of (A) SBS film, (B) PS-b-PSS-DMODA, (C) PS-*b*-PDMS and (D) PS-*b*-P2VP film after SVA-SS. The inset FFT illustrates the orientation of the cylinders.

Conclusions

We investigate the degree of the SIS nanostructure alignment using SVA-SS method as a function of annealing time; PDMS deswelling rate and PDMS swelling ratio. The Herman's orientation factor increases with increasing SVA-SS annealing time up to a threshold time (~1 h). Slower PDMS deswelling rate can also improve the alignment of the thin films, which suggests the alignment is induced by the contraction of PDMS pad during solvent removal. Furthermore, the swelling behavior of PDMS can affect the SIS nanostructures after SVA-SS significantly. By increasing the swelling of PDMS from 22% to 50% by the solvent vapor, the orientation factor can be improved from 0.67 to 0.98 and the defect density decreases from ~60 μm^{-2} to ~1 μm^{-2}. Moreover, this method has been extended to align SBS, PS-*b*-PDMS, PS-*b*-P2VP block copolymer and ionic block copolymer PS-*b*-PSS-DMODA in thin films. This investigation for understanding the mechanism of SVA-SS and its extensibility suggests that SVA-SS is a generalizable method for the alignment of BCP thin films and may be potentially applied to align other multiphase systems in films such as polymer blends or nanocomposites.

Acknowledgements

The authors acknowledge Kraton Polymers for donation of the SIS and SBS materials. JG acknowledges support from the National Science Foundation under Grant No. EEC-1161732.

Notes and references

[a] Department of Polymer Engineering, University of Akron, Akron, OH 44325. Email: vogt@uakron.edu (B.D.V.) kac25@uakron.edu (K.A.C.)

[b] Marlington High School, 10450 Moulin Ave NE, Alliance, OH 44601

Electronic Supplementary Information (ESI) available: Including AFM phase images of as-cast SIS film; Defect analysis of AFM phase images of SIS film with different PDMS pad; AFM phase images of SIS film after SVA and SVA-SS using hexane and acetone respectively; AFM phase images of PS-*b*-PSS-DMODA, PS-*b*-PMMA, PS-*b*-P2VP and PS-*b*-PDMS after standard SVA and AFM phase images of PS-*b*-PMMA after SVA and SVA-SS. See DOI: 10.1039/b000000x/

1. Soo, P. P.; Huang, B. Y.; Jang, Y. I.; Chiang, Y. M.; Sadoway, D. R.; Mayes, A. M. *J.Electrochem. Soc* **1999,** 146, (1), 32-37.
2. Xiao, Q.; Wang, X.; Li, W.; Li, Z.; Zhang, T.; Zhang, H. *J. Membr. Sci* **2009,** 334, (1-2), 117-122.
3. Segalman, R. A.; McCulloch, B.; Kirmayer, S.; Urban, J. J. *Macromolecules* **2009,** 42, (23), 9205-9216.
4. Botiz, I.; Darling, S. B. *Mater. Today* **2010,** 13, (5), 42-51.
5. Ruiz, R.; Kang, H.; Detcheverry, F. A.; Dobisz, E.; Kercher, D. S.; Albrecht, T. R.; de Pablo, J. J.; Nealey, P. F. *Science* **2008,** 321, (5891), 936-939.
6. Park, S.-M.; Liang, X.; Harteneck, B. D.; Pick, T. E.; Hiroshiba, N.; Wu, Y.; Helms, B. A.; Olynick, D. L. *ACS Nano* **2011,** 5, (11), 8523-8531.
7. Stoykovich, M. P.; Muller, M.; Kim, S. O.; Solak, H. H.; Edwards, E. W.; de Pablo, J. J.; Nealey, P. F. *Science* **2005,** 308, (5727), 1442-1446.
8. Yang, S. Y.; Ryu, I.; Kim, H. Y.; Kim, J. K.; Jang, S. K.; Russell, T. P. *Adv. Mater* **2006,** 18, (6), 709-712.
9. Jackson, E. A.; Hillmyer, M. A. *ACS Nano* **2010,** 4, (7), 3548-3553.
10. Albert, J. N. L.; Epps, T. H. *Mater. Today* **2010,** 13, (6), 24-33.
11. Bates, F. S.; Schulz, M. F.; Khandpur, A. K.; Forster, S.; Rosedale, J. H.; Almdal, K.; Mortensen, K. *Faraday Discuss* **1994,** 98, 7-18.
12. Matsen, M. W.; Thompson, R. B. *J. Chem. Phys* **1999,** 111, (15), 7139-7146.
13. Matsen, M. W.; Bates, F. S. *Macromolecules* **1996,** 29, (4), 1091-1098.
14. Bates, F. S. *Science* **1991,** 251, (4996), 898-905.
15. Knoll, A.; Horvat, A.; Lyakhova, K. S.; Krausch, G.; Sevink, G. J. A.; Zvelindovsky, A. V.; Magerle, R. *Phys. Rev. Lett* **2002,** 89, (3), 035501.
16. Knoll, A.; Magerle, R.; Krausch, G. *J. Chem. Phys* **2004,** 120, (2), 1105-1116.
17. Luo, M.; Seppala, J. E.; Albert, J. N. L.; Lewis, R. L., III; Mahadevapuram, N.; Stein, G. E.; Epps, T. H., III. *Macromolecules* **2013,** 46, (5), 1803-1811.
18. Sivaniah, E.; Hayashi, Y.; Iino, M.; Hashimoto, T.; Fukunaga, K. *Macromolecules* **2003,** 36, (16), 5894-5896.
19. Harrison, C.; Cheng, Z. D.; Sethuraman, S.; Huse, D. A.; Chaikin, P. M.; Vega, D. A.; Sebastian, J. M.; Register, R. A.; Adamson, D. H. *Phys Rev E* **2002,** 66, (1), 011706.
20. Lodge, T. P. *Macromol. Chem. and Phys* **2003,** 204, (2), 265-273.
21. RamachandraRao, V. S.; Gupta, R. R.; Russell, T. P.; Watkins, J. J. *Macromolecules* **2001,** 34, (23), 7923-7925.
22. Helfand, E.; Wasserman, Z. R. *Macromolecules* **1976,** 9, (6), 879-888.
23. Kim, S. H.; Misner, M. J.; Xu, T.; Kimura, M.; Russell, T. P. *Adv. Mater* **2004,** 16, (3), 226-231.
24. Sinturel, C.; Vayer, M.; Morris, M.; Hillmyer, M. A. *Macromolecules* **2013,** 46, (14), 5399-5415.
25. Lodge, T. P.; Dalvi, M. C. *Phys. Rev. Lett.* **1995,** 75, (4), 657-660.
26. Peng, J.; Kim, D. H.; Knoll, W.; Xuan, Y.; Li, B. Y.; Han, Y. C. *J. Chem Phys* **2006,** 125, (6), 064702.
27. Guo, R.; Huang, H.; Chen, Y.; Gong, Y.; Du, B.; He, T. *Macromolecules* **2008,** 41, (3), 890-900.
28. Albert, J. N. L.; Bogart, T. D.; Lewis, R. L.; Beers, K. L.; Fasolka, M. J.; Hutchison, J. B.; Vogt, B. D.; Epps, T. H. *Nano Lett* **2011,** 11, (3), 1351-1357.
29. Jeong, J. W.; Park, W. I.; Kim, M.-J.; Ross, C. A.; Jung, Y. S. *Nano Lett* **2011,** 11, (10), 4095-4101.

30. Qiang, Z.; Xue, J.; Cavicchi, K. A.; Vogt, B. D. *Langmuir* **2013,** 29, (10), 3428-3438.
31. Albert, J. N. L.; Young, W. S.; Lewis, R. L.; Bogart, T. D.; Smith, J. R.; Epps, T. H. *ACS Nano* **2012,** 6, (1), 459-466.
32. Morkved, T. L.; Lu, M.; Urbas, A. M.; Ehrichs, E. E.; Jaeger, H. M.; Mansky, P.; Russell, T. P. *Science* **1996,** 273, (5277), 931-933.
33. Thurn-Albrecht, T.; DeRouchey, J.; Russell, T. P.; Jaeger, H. M. *Macromolecules* **2000,** 33, (9), 3250-3253.
34. Raman, V.; Bose, A.; Olsen, B. D.; Hatton, T. A. *Macromolecules* **2012,** 45, (23), 9373-9382.
35. Segalman, R. A.; Yokoyama, H.; Kramer, E. J. *Adv.Mater.* **2001,** 13, (15), 1152-1155.
36. Angelescu, D. E.; Waller, J. H.; Adamson, D. H.; Deshpande, P.; Chou, S. Y.; Register, R. A.; Chaikin, P. M. *Adv. Mater* **2004,** 16, (19), 1736-1740.
37. Marencic, A. P.; Adamson, D. H.; Chaikin, P. M.; Register, R. A. *Phys. Rev. E* **2010,** 81, (1), 011503.
38. Tang, C.; Wu, W.; Smilgies, D.-M.; Matyjaszewski, K.; Kowalewski, T. *J. Am. Chem. Soc* **2011,** 133, (30), 11802-11809.
39. Singh, G.; Yager, K. G.; Smilgies, D.-M.; Kulkarni, M. M.; Bucknall, D. G.; Karim, A. *Macromolecules* **2012,** 45, (17), 7107-7117.
40. Singh, G.; Yager, K. G.; Berry, B.; Kim, H.-C.; Karim, A. *ACS Nano* **2012,** 6, (11), 10335-10342.
41. Xue, J. C.; Singh, G.; Qiang, Z.; Yager, K. G.; Karim, A.; Vogt, B. D. *Nanoscale* **2013,** 5, (24), 12440-12447.
42. Hong, S. W.; Huh, J.; Gu, X.; Lee, D. H.; Jo, W. H.; Park, S.; Xu, T.; Russell, T. P. *Proc. Natl. Acad. Sci USA* **2012,** 109, (5), 1402-1406.
43. Keen, I.; Yu, A.; Cheng, H.-H.; Jack, K. S.; Nicholson, T. M.; Whittaker, A. K.; Blakey, I. *Langmuir* **2012,** 28, (45), 15876-15888.
44. Jeong, J. W.; Hur, Y. H.; Kim, H.-J.; Kim, J. M.; Park, W. L.; Kim, M. J.; Kim, B. J.; Jung, Y. S. *ACS Nano* **2013,** 7, (8), 6747-6757.
45. Qiang, Z. Zhang, L.; Stein, G.E. Cavicchi, K.A; Vogt, B.D. *Macromolecules* **2014,** 47, (3), 1109-1116.
46. Wadley, M. L.; Cavicchi, K. A. *J.Appl. Polym. Sci.* **2010,** 115, (2), 635-640.
47. Lee, J. N.; Park, C.; Whitesides, G. M. *Anal Chem* **2003,** 75, (23), 6544-6554.
48. Herzinger, C. M.; Johs, B.; McGahan, W. A.; Woollam, J. A.; Paulson, W. *J. Appl. Phys* **1998,** 83, (6), 3323-3336.
49. Lodge, T. P.; Pan, C.; Jin, X.; Liu, Z.; Zhao, J.; Maurer, W. W.; Bates, F. S. *J. Polym Sci B* **1995,** 33, (16), 2289-2293.
50. Khandpur, A. K.; Forster, S.; Bates, F. S.; Hamley, I. W.; Ryan, A. J.; Bras, W.; Almdal, K.; Mortensen, K. *Macromolecules* **1995,** 28, (26), 8796-8806.
51. Choi, K. J.; Spruiell, J. E.; White, J. L. *J. Polym Sci B* **1982,** 20, (1), 27-47.
52. Marencic, A. P.; Adamson, D. H.; Chaikin, P. M.; Register, R. A. *Phys Rev E* **2010,** 81, (1), 10, 011503.
53. Palchesko, R. N.; Zhang, L.; Sun, Y.; Feinberg, A. W. *Plos One* **2012,** 7, (12), e51499.
54. Tong, Q.; Sibener, S. J. *Macromolecules* **2013,** 46, (21), 8538-8544.
55. Ye, C.; Singh, G.; Wadley, M.L.; Karim, A.; Cavicchi, K.A.; Vogt, B.D. *Macromolecules* **2013,** 46, (21), 8608-8615.
56. Russell, T. P.; Hjelm, R. P.; Seeger, P. A. *Macromolecules* **1990,** 23, (3), 890-893.
57. Zhao, Y.; Sivaniah, E.; Hashimoto, T. *Macromolecules* **2008,** 41, (24), 9948-9951.